Functional Design of Textiles and Development of Cultural and Creative Products

Jing Huang
School of Art, Wuxi Taihu University, Wuxi 214063, Jiangsu, China
Corresponding author: Jing Huang (e-mail: 18851515083@163.com)

ABSTRACT The integration of functional textiles with cultural and creative products requires not only aesthetic preservation but also intelligent thermal management and reliable electrothermal performance. Such requirements are increasingly relevant to flexible electronic systems and electromagnetic applications, where stable conductive pathways and thermal regulation are essential for device reliability. This study proposes an intelligent cultural scroll based on a Tang Dynasty Baoxianghua pattern by integrating graphene-based conductive textiles, topology-optimized microcircuit design, and fuzzy proportional–integral–derivative (PID) temperature control. The cultural pattern is first transformed into an optimized conductive topology to minimize temperature deviation while preserving its artistic characteristics. Graphene conductive ink is subsequently screen-printed onto textile substrates and encapsulated through a hot-pressing process to form flexible electrothermal circuits, followed by the integration of temperature sensing and adaptive closed-loop control. Experimental results demonstrate that the fabricated heating unit reaches 50 °C within 80 s under a safe 5 V supply, while topology optimization reduces the maximum surface temperature difference from 19.4 °C to 1.1 °C. After external thermal disturbances, the fuzzy PID controller restores the target temperature within 25 s, exhibiting excellent robustness and stability. The proposed strategy provides an effective approach for combining cultural design with intelligent electrothermal textiles and offers valuable insights for flexible electromagnetic devices, wearable electronic systems, and thermally regulated functional materials requiring uniform current distribution and reliable energy management.

INDEX TERMS functional textiles, graphene heating fabrics, electrothermal optimization, fuzzy PID control, flexible electromagnetic devices

I. INTRODUCTION

As a crucial carrier of culture, the integration of textiles with cultural and creative products is an effective way to preserve and innovate cultural heritage. Applying functional design concepts to the development of cultural and creative textiles not only enhances the practical value and user experience of products but also expands the boundaries of the integration of traditional craftsmanship and modern technology, providing new approaches and technical support for the preservation and innovation of cultural heritage [1,2]. This interdisciplinary research field has significant academic value and broad application prospects.

Currently, the development of cultural and creative products for the display and preservation of high-end calligraphy and painting faces key challenges: on the one hand, there is a contradiction between functional empowerment and aesthetic expression. Conventional heating materials such as metal wire or carbon fiber are difficult to integrate with delicate cultural patterns, often sacrificing the integrity of the pattern in exchange for functionality, which undermines the artistic quality of the product [3,4]. On the other hand, the challenges of precise and safe thermal management are prominent. Achieving large-scale, uniform, and stable low-temperature heating while avoiding local overheating places extremely high demands on circuit design and control strategies [5,6]. In addition, the product's flexibility, durability, and compatibility with cultural media are insufficient. Many functional treatments make the fabric stiff or affect its drape, making it difficult to meet the material texture requirements of specific cultural and creative forms such as scrolls [7,8]. To overcome the above contradictions, existing research has attempted a variety of technical paths, but all have obvious limitations. Functional finishing processes such as coating are used to give fabrics heating properties, but this method has the disadvantages of poor coating uniformity, hardened feel, and insufficient water washing durability [9,10]. Conductive yarns are embroidered on the surface of fabrics using embroidery technology to form circuits. Although this method can form patterns, the circuit resistance is high, the thermal efficiency is low, and the embroidery nodes are prone to become failure points [11,12]. Although solutions based on flexible printed circuit boards can achieve precise control, their rigid substrate is incompatible with the soft texture of textiles, which destroys the user experience [13]. Overall, these methods have failed to achieve a cohesive combination of cultural patterns, efficient heating, flexible fabric substrates, and intelligent control.

To address the above challenges, this paper proposes a method for developing smart scrolls based on graphene ink screen printing and topology optimization circuit design, achieving a systematic integration of cultural aesthetics and heating functions from both the physical structure and control system levels. This method first performs vector graphics analysis on the selected cultural patterns, and applies a topology optimization algorithm driven by Joule heat simulation to reconstruct the electrothermal performance of their line widths and paths; then, highly conductive graphene ink is used to precisely print the optimized pattern on the fabric through screen printing technology, and the pattern is packaged through a low-temperature hot pressing composite process; finally, a micro temperature sensor is integrated and a fuzzy proportional integral differential control algorithm is deployed to achieve closed-loop temperature control. By seamlessly embedding intelligent heating units into cultural patterns and achieving precise temperature control at the system level, this study provides a new design paradigm and theoretical basis for the high-value-added, high-tech innovation of cultural and creative products.

II. INTELLIGENT SCROLL CONSTRUCTION METHOD BASED ON CULTURAL PATTERNS

A. CIRCUIT FUNCTIONAL TRANSLATION AND VECTOR ANALYSIS OF CULTURAL PATTERNS

To achieve a deep integration of cultural patterns and functional heating circuits, the first step is to transform the aesthetic pattern into a basic geometric path for subsequent electrical optimization and physical manufacturing. This study selects the typical Baoxianghua pattern of the Tang Dynasty as a cultural carrier. Its full composition, smooth lines, and high symmetry are conducive to the construction of a continuous and balanced conductive circuit. To achieve high-precision digitization, the Baoxianghua pattern is first digitized with high-precision vectors: the vector analysis process of the pattern begins with the input of a high-definition image of the Baoxianghua. The active contour line model based on the gradient vector flow field is used to automatically identify and finely extract the contours of the core pattern elements such as the petals and leaves of the Baoxianghua [14,15]. The model drives the curve $C(s)$ to fit the edge of the pattern by minimizing the energy functional E_{total}, as shown in formula (1):

$$E_{total} = \int_0^1 \left[\alpha \left|C'(s)\right|^2 + \beta \left|C''(s)\right|^2 + E_{ext}\left(C(s)\right)\right] ds \tag{1}$$

In formula (1), E_{ext} is composed of image gradient information, which drives the curve to fit the edge of the pattern; α and β are weight coefficients that control the smoothness of the curve. The output of this process is a set of closed Bezier curves $\{C_i\}$ that describe the outline of each unit pattern of the Baoxianghua. These vector paths ensure that the extracted pattern remains smooth and lossless under any scaling, providing an accurate geometric basis for subsequent circuit design. To achieve the transformation of pattern elements into circuit functional units, the central axis of each outline is then mapped to the initial circuit path $\{P_j\}$ through a morphological skeleton extraction algorithm. That is, cultural elements such as the “petal” outline are clearly defined as the initial conductive channel and given an initial line width W_j. The initial resistance $R_{initial}$ of the path is theoretically estimated by the resistance formula of a uniform cross-section conductor:

$$R_{initial} = \rho \frac{L_j}{W_j \cdot H} \tag{2}$$

In formula (2), ρ is the volume resistivity of the preset graphene ink, L_j is the geometric length of path P_j, W_j is the initial line width assigned by the mapping, and H is the preset printed film thickness. This initial resistance estimate provides the starting point for electrical performance iteration for subsequent topology optimization. Thus, the cultural pattern has completed the transformation from a visual symbol to a functional geometric configuration with a preliminary electrical model. A clear mapping relationship has been established from cultural elements such as “petals” and “branches and leaves” to the circuit functional unit of “conductive path”, laying the foundation for input conditions that combine cultural attributes and functional objectives for performance-driven circuit optimization.

B. PATTERN-CIRCUIT TOPOLOGY COLLABORATIVE OPTIMIZATION FOR THERMAL FIELD UNIFORMITY

The initial circuit path obtained only has a geometric shape, and its electrothermal performance is often poor. Direct use for heating will result in severe temperature unevenness. To eliminate the hot spot effect of the initial circuit, a variable density method is used for topology optimization. The pseudo-density ρ_e of the finite element mesh unit is used as the design variable, and its physical conductivity is interpolated through the penalty model $\sigma_e = \sigma_{max}\rho_e^3$. The direct primary objective of the topology optimization is to minimize the standard deviation of the temperature distribution, as defined in Formula (3). Uniform current density distribution is the underlying physical mechanism responsible for improved thermal uniformity.

$$\min : F = \sqrt{\frac{1}{N}\sum_{i=1}^{N}\left(T_i - \overline{T}\right)^2} \tag{3}$$

In formula (3), T_i is the unit temperature, $\overline{T}$ is the average temperature, and N is the total number of units. Under constant voltage excitation, by solving the Joule thermal coupling field and using sensitivity analysis to guide iteration, the equivalent line width of each region (i.e., material distribution) is automatically adjusted to make the current path tend to be balanced [16]. The optimized circuit retains the pattern topology characteristics while effectively improving the thermal field uniformity. The effect of the optimization process is intuitively presented by comparing the initial and optimized simulated circuit geometry and its simulated thermal field distribution. The brief simulation results are shown in Figure 1.

Figure 1 compares the simulated circuit layout and the simulated thermal field before and after topology optimization, visually presenting the optimization effect based on the thermal uniformity goal. Sub-figures (a) and (b) illustrate that the sharp corners of the initial layout lead to current density concentration, forming local high-temperature hotspots exceeding 85 °C, and the thermal field distribution is extremely uneven. Subfigures (c) and (d) illustrate that the optimized circuit uses smooth corners and smoothly varying line widths, effectively balancing the current path, controlling the maximum temperature to within approximately 68 °C, and significantly improving the uniformity of the thermal field distribution. This comparison verifies the effectiveness of the topology optimization algorithm in coordinating the aesthetic requirements of cultural patterns with functional heating performance, laying a theoretical foundation for subsequent physical preparation.

C. IN-SITU FABRICATION OF GRAPHENE CIRCUITS BASED ON SCREEN PRINTING

The optimized circuit topology must be transformed into a physical entity through functional materials. This study employs screen printing technology, and its successful implementation relied on the preparation of a high-performance graphene composite conductive ink. The ink utilizes highly conductive graphene powder as the functional phase, a water-based polyurethane resin as the binder, and additives such as dispersants and leveling agents. The ratio of these components directly influences the ink's conductivity, printability, and mechanical properties after film formation [17,18]. After precise weighing, the ink is initially mixed using a high-speed shear emulsifier at 2000 rpm. The mixture is then cyclically ground in a three-roll mill at a specific roller gap and pressure for at least five cycles until the slurry reaches a fineness of less than 15 μm, ensuring sufficient dispersion of the graphene and the formation of a conductive network. The key performance parameters and formulation of the ink are shown in Table 1.

TABLE 1. Graphene conductive ink formulation and key performance parameters

Composition/Performance parameters	Value	Description
Graphene solid content (wt%)	25 ± 2	Conductive functional phase
Waterborne polyurethane resin (wt%)	35 ± 2	Binder, providing adhesion
Dispersant (wt%)	3 ± 0.5	Improve graphene dispersion stability
Viscosity (mPa·s, 25 °C)	4500 ± 500	Brookfield viscometer measurement
Solid content (%)	55 ± 3	Affects drying rate and film thickness
Square resistance after sintering	≤ 0.5	Key electrical performance indicators

The printing process uses a 300-mesh polyester screen, which provides a reliable printing resolution for a minimum feature size (line width) of approximately 100 μm. This capability ensures that the subtle width variations generated by the topology optimization algorithm can be accurately reproduced in the physical circuit. A scraper pushes the ink across the screen at a 60° angle, constant speed, and pressure, allowing it to precisely deposit through the mesh onto the polyester base fabric. The rheological behavior of the ink follows the modified Bingham model, with the relationship between shear stress τ and shear rate γ being shown in formula (4):

$$\tau = \tau_0 + k\gamma^n \tag{4}$$

In formula (4), τ_0 is the yield stress, the minimum stress required for the ink to begin flowing; k is the consistency coefficient; and n is the flow index. This rheological property ensures that the ink's viscosity decreases under the shearing action of the scraper, allowing it to easily pass through the mesh. Once deposited on the base fabric, the viscosity quickly recovers (thixotropy), preventing pattern seepage and diffusion, thereby achieving clear circuit boundaries. The printed samples are sintered in a forced-air drying oven at 120 °C for 15 minutes to crosslink and cure the resin, forming a strong and conductive functional coating. This process transforms the optimized digital circuit model into a functional physical entity attached to the textile.

D. FLEXIBLE SYSTEM INTEGRATION AND PACKAGING PROTECTION

The graphene circuits formed by printing and sintering need to be encapsulated and protected to achieve stable application. This study uses a hot pressing process to laminate a 50-micron-thick thermoplastic polyurethane film to a textile substrate printed with circuits. The hot pressing process is carried out under specific temperature, pressure, and time conditions. Its core mechanism is that the surface layer of the Thermoplastic Polyurethane (TPU) film is heated and melted, and under the action of pressure, it penetrates into the gap between the graphene conductive layer and the

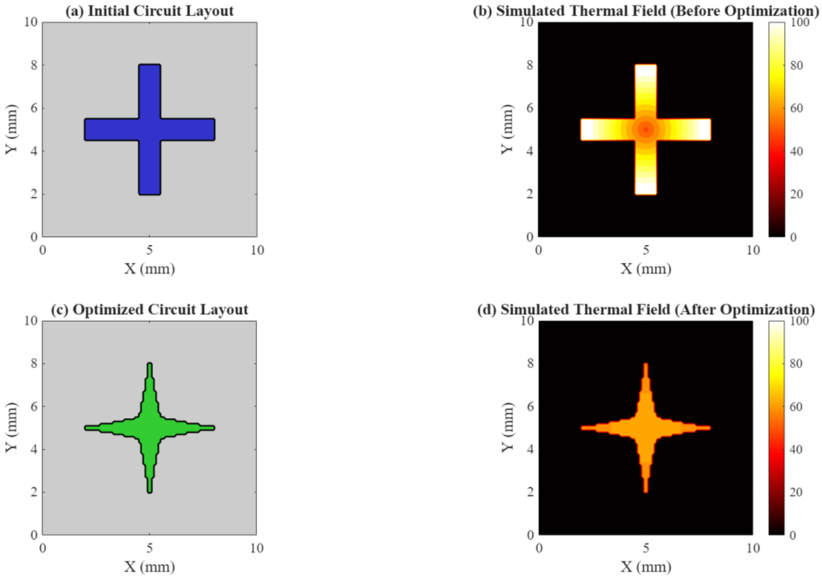

FIGURE 1. Comparison of circuit topology before and after optimization (a) Initial layout; (b) Simulated thermal field before optimization; (c) Optimized circuit layout; (d) Simulated thermal field after optimization

textile fibers, achieving mechanical interlocking and physical encapsulation. The peel strength Fb of this laminated structure can be approximately characterized as:

$$F_b = g\sqrt{\frac{E \cdot W}{\delta}} \tag{5}$$

In formula (5), E represents the elastic modulus of the TPU film, W is the interface binding energy, δ is the characteristic size of the interface defect, and g is the proportional coefficient related to the process conditions. Higher hot pressing temperature and pressure help increase the binding energy W and reduce the defect size δ, thereby improving the peel strength F_b and ensuring that the packaging layer does not fall off under stress such as bending and washing. After the packaging is completed, the flexible insulated wire is connected to the preset electrode area of the circuit using conductive silver glue, and reinforced by dispensing. A digital temperature sensor is integrated at the geometric center of the heating area for closed-loop control. This single-point sensing strategy is justified because the topology optimization ensures a highly uniform temperature distribution, making the central temperature a reliable feedback signal for the control system. The sensor's data pin is connected to the single-bus interface of the microcontroller unit. The microcontroller has a built-in fuzzy proportional integral differential control algorithm. The algorithm uses the deviation e between the actual temperature read by the sensor and the set temperature and the deviation change rate ec as the input of the fuzzy inference system. By querying the fuzzy rule table based on expert experience, the duty cycle adjustment value Δu of the PWM (Pulse Width Modulation) signal is output in real time. The quantized ranges (universe of discourse) for the fuzzy inputs were set as: temperature deviation (e) from -10 °C to +10 °C, deviation change rate (ec) from -5 °C/s to +5 °C/s. The output, PWM duty cycle adjustment (Δu), was defined in the range of -20% to +20%. The fuzzy inference process is as follows:

$$\Delta u = \mathrm{Fuzzify}(e, ec) \circ R \tag{6}$$

In formula (6), Fuzzify represents the fuzzy processing of the precise input, R represents the fuzzy rule relationship matrix, and $\circ$ is the fuzzy synthesis operator. The final output PWM signal drives the MOSFET power switch tube, adjusting the average voltage applied to the heating circuit, forming a complete closed-loop intelligent temperature control system, which accurately maintains the surface temperature of the scroll within the set range.

III. SMART SCROLL PERFORMANCE TESTING AND FUNCTION VERIFICATION

A. EXPERIMENTAL MATERIALS AND SAMPLE PREPARATION

The experimental substrate used is 220T plain-weave polyester fabric with an areal density of 80 g/m2 and warp and weft densities of 120 and 80 strands/cm, respectively. The conductive ink's main components include a water-based polyurethane resin with a 40% solids content, graphene powder with a flake size of 5–10 μm, and a dispersant and defoamer to adjust rheological properties. The encapsulation material is a 50 μm-thick thermoplastic polyurethane film with a melt index of 25 g/10 min (tested at 190 °C/2.16 kg). The control system hardware core utilizes an STM32F103C8T6 microcontroller, a DS18B20 digital sensor for temperature sensing, and an IRF3205 MOSFET for power drive.

Sample preparation: First, the Baoxianghua pattern is vector analyzed and topologically optimized to generate the photolithography file of the final circuit pattern. Subsequently, a 300-mesh polyester screen is used to print the prepared graphene conductive ink on a polyester base fabric on an automatic screen printer. The printed sample is placed in a 120 °C forced air drying oven for curing for 15 minutes to form a conductive path. Then, the TPU film is covered on the surface of the printed circuit and hot-pressed in a hot press at 150 °C and 0.5 MPa pressure for 90 seconds to complete the encapsulation. Finally, conductive silver glue is used to connect the Flexible Printed Circuit (FPC) wire as an electrode, and the temperature sensor is fixed at the geometric center of the heating area and electrically connected to the microcontroller module. To investigate the impact of key parameters, five groups of samples are prepared: S-1 is a standard sample (line width 1.0 mm), S-2 and S-3 are comparative samples with line widths of 0.8 mm and 1.2 mm, respectively, S-4 is a sample with a 10% increase in graphene content, and S-5 is a sample with a hot-pressing temperature adjusted to 130 °C. All samples are prepared under the same environmental conditions to ensure comparability of the experimental results. The peel strength, a key indicator of encapsulation quality, was measured for representative samples. The standard sample S-1 exhibited a peel strength of 3.8 N/cm, while sample S-5, processed at the lower hot-pressing temperature, showed a significantly reduced value of 1.2 N/cm.

The topology optimization, by adjusting the equivalent line width, effectively modifies the cross-sectional area of the current path, thereby altering the overall circuit resistance. For the standard sample S-1, the initial theoretical resistance estimated by Equation (2) was 18.5 Ω. After optimization and fabrication, the measured steady-state resistance of the physical circuit was 23.1 Ω. This finalized resistance value is the fundamental parameter used in all subsequent electrothermal performance testing and analysis.

B. TEST INSTRUMENTS AND METHODS

To systematically evaluate the comprehensive performance of the prepared intelligent heating scroll sample, three major test categories are established based on its functional application scenarios: electrothermal performance, mechanical durability, and intelligent temperature control accuracy. The instrumentation and key parameters required for these tests are as follows: Electrical performance testing is performed using a Keysight 34465A digital multimeter; thermal performance testing is performed using a FLIR A655sc infrared thermal imager with a thermal sensitivity of 0.03 °C; environmental testing is conducted in a Binder KBF240 constant temperature and humidity chamber; mechanical durability testing is performed using an Instron 3345 universal materials testing machine; and temperature control accuracy testing is performed using the microcontroller's built-in ADC (Analog-to-Digital Converter) module, with data recorded synchronously with the host computer software. The specific performance test items and method standards are shown in Table 2.

Table 2 systematically lists the complete test plan for verifying sample performance. The electrothermal performance test verifies the effectiveness of the topology optimization and printing process; the mechanical durability test evaluates the reliability of the packaging layer under simulated operational stress; and the intelligent temperature control test directly verifies the actual control effectiveness of the fuzzy PID algorithm. All tests are conducted under standard atmospheric conditions of 23 ± 2 °C and 50 ± 5% relative humidity. Each test is repeated at least three times, and the average value is taken to ensure data reliability. This test system provides a comprehensive and quantifiable data foundation for the results and analysis in Chapter 4.

IV. RESULTS AND DISCUSSION: VERIFICATION OF THE IMPLEMENTATION EFFECT OF FUNCTIONAL DESIGN

A. ANALYSIS OF HIGH-EFFICIENCY ELECTRIC HEATING PERFORMANCE

The practical application of smart heating fabrics lies in their electrothermal conversion efficiency and response speed. This section aims to quantitatively evaluate the steady-state operating temperature and dynamic temperature rise of topologically optimized graphene circuits under different design parameters to verify the effectiveness of the functional design. Key dynamic thermal performance parameters are obtained by applying rated voltage to samples with varying conductive line widths and simultaneously recording the changes in surface temperature and power consumption over time. The test results are shown in Figure 2.

The results in Figure 2 show that sample S-2, with a line width of 0.8 mm, exhibits the fastest heating rate and the highest steady-state temperature of 61.5 °C. This is attributed to its higher electrical resistance, which leads to increased power dissipation under constant voltage. In contrast, sample S-3, with a line width of 1.2 mm, exhibits a more gradual temperature rise, with a lower steady-state temperature of 53.1 °C. This is attributed to the increased cross-sectional area, which reduces resistance and heat generation. The standard sample S-1 (line width of 1.0 mm) maintains a stable steady-state temperature of 56.3 °C. Figure 2(b) further reveals the power dynamics of sample S-1. Initially, the power is 2.50 W. As the temperature increases, the graphene's resistance increases due to the positive temperature coefficient effect, causing the power to decrease after 100 seconds and stabilize at 2.16 W, a decrease of 13.6%. This self-regulating characteristic contributes to the thermal safety of the system. Analysis shows that circuit line width is a key design parameter for controlling thermal performance, and topology optimization requires a balance between thermal uniformity and target temperature.

TABLE 2. Performance test items and corresponding method standards

Test category	Specific test items	Core instruments and equipment	Test conditions/standards	Key evaluation indicators
Electric heating performance	Temperature rise characteristics and steady-state power	DC (Direct Current) power supply, multimeter, thermal imager	5V DC power supply, ambient temperature 25 °C	Heating curve, steady-state temperature, maximum power
Electric heating performance	Surface temperature uniformity	Infrared thermal imager	After reaching steady state, shoot at a vertical distance of 30cm	Temperature standard deviation, thermal field distribution map
Mechanical durability	Bending fatigue	Customized bend tester	Curvature radius 10mm, cycle frequency 1Hz, 1000 times	Resistance change rate ($\Delta R/R_0$)
Mechanical durability	Adhesion fastness	Universal material testing machine	180° peeling, tensile speed 100 mm/min	Average peel strength (N/cm)
Intelligent temperature control	Constant temperature accuracy and stability	Microcontroller, temperature sensor	Set the target temperature to 50 °C and the ambient temperature fluctuation to ±2 °C	Temperature fluctuation range, overshoot

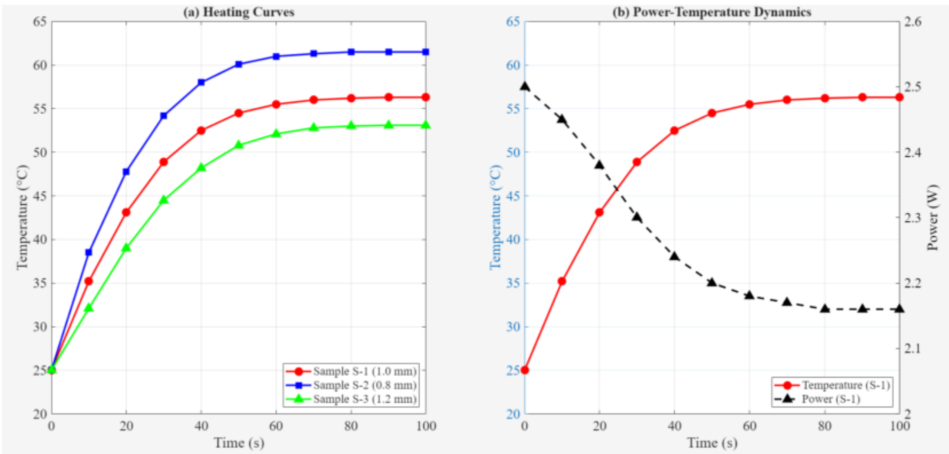

FIGURE 2. Dynamic thermal performance results under different parameters (a) time-temperature; (b) time-power at S-1 temperature

B. ANALYSIS OF THERMAL FIELD UNIFORMITY AND SAFETY PERFORMANCE EVALUATION OF HEATING SURFACES

Heating uniformity is a key performance metric for functional heating fabrics and directly impacts product safety and user experience. This section focuses on the surface temperature distribution of a topology-optimized circuit under actual operating conditions, verifying the effectiveness of the optimization algorithm in improving thermal field uniformity. Infrared thermal imaging technology is used to scan the surface of a sample in steady-state operation, extracting temperature data along specific paths for quantitative analysis. The results are shown in Figure 3.

The results in Figure 3 show that the simulation temperature curve before topology optimization showed large fluctuations, with a peak of 72.5 °C at the 0 mm position of the measurement path and a minimum of 53.1 °C at 5 mm, with a temperature peak difference of up to 19.4 °C. This unevenness is due to the sharp corners and width mutations in the initial circuit path, which lead to excessive local current density and the formation of hot spots. After topology optimization, the measured temperature distribution tends to be flat, and the temperature difference between the highest 56.3 °C and the lowest 55.2 °C is only 1.1 °C. The optimization algorithm effectively balances the resistance distribution of the current path by smoothing the path contour and adjusting the line width distribution, thereby suppressing local overheating. The analysis results show that the topology optimization design based on thermal field uniformity can effectively improve the temperature distribution performance of the heating fabric.

C. ANALYSIS OF FLEXIBILITY, DURABILITY AND PRODUCT APPLICABILITY

The durability of flexible electronic devices is a key challenge in their practical application. This section systematically evaluates the mechanical stability and reliability of a graphene heating circuit and its packaging structure by simulating the repeated bending stresses that a scroll painting might experience during use. Samples prepared using different hot-pressing composite process parameters are subjected to a specified frequency of bending fatigue testing, and the degradation of their electrical and thermal functions is monitored. The relevant performance changes are shown in Figure 4.

The results in Figure 4 show that after 1000 bending cycles, the resistance change of the standard sample S-1 is 14.5%, while the resistance change of the sample S-5, which

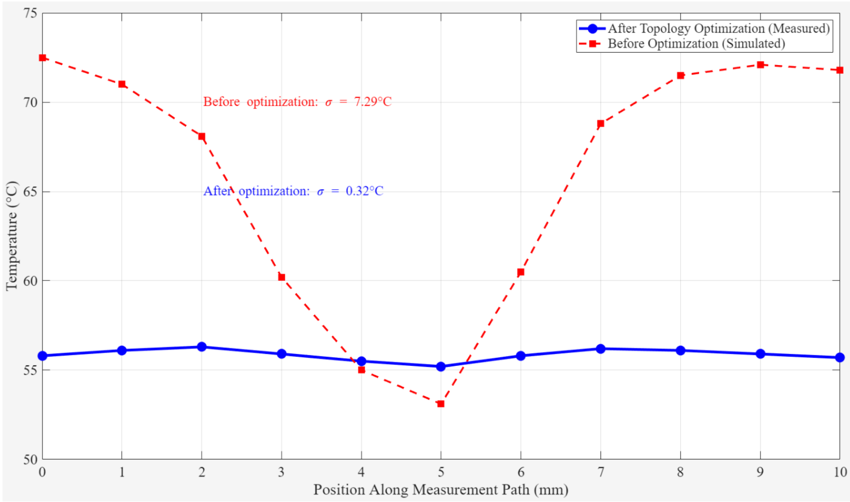

FIGURE 3. Surface temperature distribution results

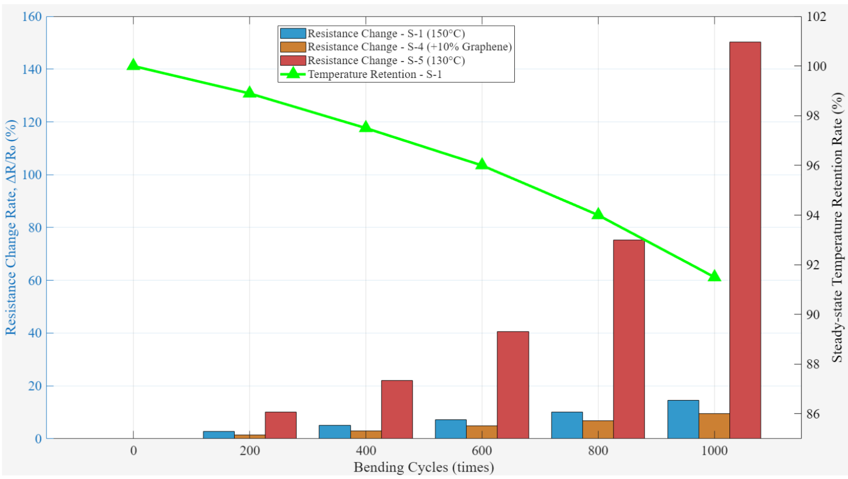

FIGURE 4. Flexible durability and stability results at different cycle times

is hot-pressed at a lower temperature, increased dramatically to 150.2%. At the lower temperature, the encapsulation layer of the S-5 sample failed to fully fuse the TPU molecules with the fabric substrate and the conductive circuit, resulting in weak interfacial bonding. This results in microcracks that easily formed and rapidly propagated under mechanical stress, causing the conductive pathway to break. In contrast, the resistance change of sample S-4, which has a 10% increase in graphene content in the ink, is 9.5%, demonstrating superior conductive durability compared to the standard sample. This is attributed to the higher graphene content forming a denser and more redundant three-dimensional conductive network after the ink cures. When local pathways are damaged by mechanical stress, current can be transmitted through more alternative pathways, thereby slowing the increase in overall resistance. Correspondingly, the steady-state temperature retention of the S-1 sample drops from 100% to 91.5%, indicating a negative correlation between performance degradation and resistance increase, consistent with Ohm's law and Joule heating. The simultaneous decay of electrical and thermal properties confirms the crucial role of the encapsulation process in maintaining the structural integrity of the functional layer. Analysis shows that an optimized hot-pressing composite process is key to ensuring the long-term operational reliability of smart heating textiles.

D. VERIFICATION OF INTELLIGENT TEMPERATURE CONTROL ACCURACY AND SYSTEM ROBUSTNESS

The accuracy and robustness of intelligent temperature control systems directly determine the practical value of functional textiles. This section examines the comprehensive performance of a control system based on the fuzzy PID algorithm in terms of dynamic response, steady-state maintenance, and interference rejection by constructing a test environment containing external disturbances. Temperature data and control signal changes are recorded throughout the system's startup, steady-state, application of disturbances, and recovery. Figure 5 shows the system's response characteristics.

The results in Figure 5 show that the system reaches

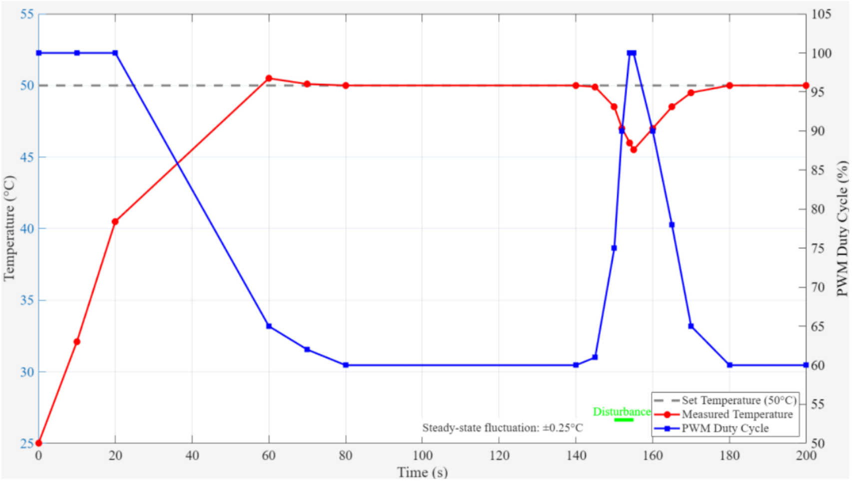

FIGURE 5. Measured temperature control and PWM duty cycle results

the set temperature of 50 °C within 80 seconds. During the heating phase, the PWM duty cycle gradually decreases from 100% to 60%, indicating that the controller dynamically adjusts based on the temperature deviation. An external disturbance applies at 150 seconds caused the temperature to drop sharply to 45.5 °C within 5 seconds. The controller then responded quickly, immediately increasing the PWM duty cycle to 100% to maximize heating power. Thanks to the fuzzy rules' effective handling of nonlinear relationships, the system stabilizes the temperature back to 50 °C within 25 seconds after the disturbance ended. This rapid recovery capability and high-precision stability stem from the fuzzy PID algorithm's comprehensive assessment of the deviation and its rate of change, which outperforms traditional PID in nonlinear systems. The test results demonstrate that the intelligent temperature control system has excellent dynamic quality and robustness.

V. CONCLUSION

This study applies topology optimization and fuzzy control algorithms to the functional design of textiles and the development of cultural and creative products, establishing a comprehensive technical pathway from cultural patterns to intelligent temperature-controlled products. Through circuit topology optimization based on thermal field uniformity, the peak temperature difference on the surface of the heating fabric is reduced from 19.4 °C before optimization to 1.1 °C, effectively eliminating the risk of localized overheating. Samples prepared using a graphene ink screen printing and hot pressing composite process maintain a resistance change rate of 14.5% for the standard sample S-1 after 1000 bending cycles, demonstrating excellent mechanical durability. An integrated fuzzy PID control system stabilizes the scroll's temperature to 50 °C within 25 seconds after the external disturbance ended, demonstrating excellent robustness. This method provides a viable approach for integrating traditional cultural elements with high-performance intelligent textile technologies. The developed intelligent constant-temperature scroll not only enhances the practical functionality and interactive experience of cultural and creative products but also offers a viable technical solution for applications such as preventative cultural heritage conservation and high-end art exhibitions, enabling textiles to evolve from passive cultural carriers to functionally augmented cultural media.

AUTHOR CONTRIBUTIONS

Jing Huang designed, collected and analyzed the data, and drafted the manuscript. Jing Huang conducted the study, critically revised the manuscript for important intellectual content, and gave final approval of the version to be published. Jing Huang participated fully in the work, take public responsibility for appropriate portions of the content, and agreed to be accountable for all aspects of the work in ensuring that questions related to the accuracy or integrity of any part of the work are appropriately investigated and resolved.

CONFLICTS OF INTEREST

The author declares no conflict of interest.

FUNDING

This research received no external funding.

ACKNOWLEDGEMENTS

Not applicable.

REFERENCES

[1] S. T. Wei, "Chinese embroidery in cultural and creative product design," Journal of Fiber and Bioengineering and Informatics, vol. 17, no. 2, pp. 89-102, 2024, doi: 10.3993/jfbim02941.

[2] L. Deng, F. Zhou, and Z. Zhang, "Interactive genetic color matching design of cultural and creative products considering color image and visual aesthetics," Heliyon, vol. 8, no. 9, Art. no. e10768, 2022, doi: 10.1016/j.heliyon.2022.e10768.

[3] M. R. Repon and D. Mikučionienė, "Progress in flexible electronic textile for heating application: A critical review," Materials, vol. 14, no. 21, pp. 6540, 2021, doi: 10.3390/ma14216540.

[4] Y. Chen, J. Hart, M. Suh, K. Mathur, and R. Yin, "Electromechanical characterization of commercial conductive yarns for e-textiles," Textiles, vol. 3, no. 3, pp. 294-306, 2023, doi: 10.3390/textiles3030020.

[5] L. Tang, B. Lyu, D. Gao, Z. Jia, Y. Fu, and J. Ma, "A Janus textile with tunable heating modes toward precise personal thermal management in cold conditions," Small, pp. 20(15), 2023, doi: 10.1002/smll.202308194.

[6] J. Li, H. Yan, Y. Ni, L. Fu, and Y. Yang, "Simulation and analysis of heat transfer performance of electrical heating fabric at low temperature based on skin tissue," International Journal of Clothing Science and Technology, vol. 35, no. 3, pp. 363-380, 2023, doi: 10.1108/IJCST-02-2022-0021.

[7] H. Zhai, J. Liu, Z. Liu, and Y. Li, "Functional graphene fiber materials for advanced wearable applications," Advanced Fiber Materials, vol. 7, no. 2, pp. 443-468, 2025, doi: 10.1007/s42765-025-00512-1.

[8] M. Shak Sadi and E. Kumpikaitė, "Advances in the robustness of wearable electronic textiles: Strategies, stability, washability and perspective," Nanomaterials, vol. 12, no. 12, pp. 2039, 2022, doi: 10.3390/nano12122039.

[9] H. N. Choi, S. H. Jee, J. Ko, D. J. Kim, and S. H. Kim, "Properties of surface heating textile for functional warm clothing based on a composite heating element with a positive temperature coefficient," Nanomaterials, vol. 11, no. 4, pp. 904, 2021, doi: 10.3390/nano11040904.

[10] S. Hu, D. Wang, D. Křemenáková, and J. Militký, "Characterization and Multifunction Application of Metalized Textile Materials," Advanced Multifunctional Materials from Fibrous Structures. Singapore: Springer Nature Singapore; 2023.

[11] Y. Zheng, L. Jin, J. Qi, Z. Liu, L. Xu, S. Hayes, et al., "Performance evaluation of conductive tracks in fabricating e-textiles by lock-stitch embroidery," Journal of Industrial Textiles, vol. 51, no. 4 Suppl, Art. no. 6864S-6883S, 2020, doi: 10.1177/1528083720937289.

[12] Y. Zhang, J. Hu, X. Yan, and H. Tu, "The equivalent resistance model of double-layer embroidered conductive lines on nonwoven fabric," Journal of Industrial Textiles, vol. 51, no. 5 Suppl, Art. no. 8565S-8581S, 2021, doi: 10.1177/15280837211049481.

[13] E. Skrzetuska and P. Rzeźniczak, "Circularity of smart products and textiles containing flexible electronics: Challenges, opportunities, and future directions," Sensors, vol. 25, no. 6, pp. 1787, 2025, doi: 10.3390/s25061787.

[14] Q. Qian, K. Cheng, W. Qian, Q. Deng, and Y. Wang, "Image segmentation using active contours with Hessianbased gradient vector flow external force," Sensors, vol. 22, no. 13, pp. 4956, 2022, doi: 10.3390/s22134956.

[15] D. Wang, X. Dang, W. Liu, and Y. Wang, "Image segmentation using active contours with image structure adaptive gradient vector flow external force," Frontiers in Applied Mathematics and Statistics, pp. 9, 2023, doi: 10.3389/fams.2023.1271296.

[16] G. Reales Gutiérrez, A. M. Aragón, H. F. L. Goosen, A. Bornheim, and F. van Keulen, "Coupled thermo-electro-mechanical topology optimization for cooling applications under electrical constraints," Structural and Multidisciplinary Optimization, pp. 68(7), 2025, doi: 10.1007/s00158-025-04087-8.

[17] I. Improta, G. Rollo, G. G. Buonocore, S. Del Ferraro, V. Molinaro, G. D'Addio, et al., "On the enhancement of the long-term washability of e-textile realized with electrically conductive graphene-based inks," Polymers, vol. 17, no. 7, pp. 904, 2025, doi: 10.3390/polym17070904.

[18] Y. Zhang, X. Chen, Y. Dong, G. Zhang, H. Cai, Y. Wu, and Y. Bai, "High-conductivity graphene/carbon black inks via interpenetrating networks for wearable fabric-based heaters and strain sensors," Journal of Materials Chemistry C, vol. 12, no. 27, pp. 10083-10095, 2024, doi: 10.1039/D4TC01100G.